From Monomers to π-Stacks. A Comprehensive Study of the Structure and Properties of Monomeric, π-Dimerized, and π-Stacked Forms of the Cation Radical of 3′,4′-Dibutyl-2,5″-diphenyl-2,2′:5′,2″-terthiophene

David D. Graf, Robert G. Duan, John P. Campbell, Larry L. Miller,* and Kent R. Mann*

Contribution from the Department of Chemistry, University of Minnesota, Minneapolis, Minnesota 55455

Received December 17, 1996[⊗]

Abstract: 3′,4′-Dibutyl-5,5″-diphenyl-2,2′:5′,2″-terthiophene (Bu_2Ph_2Tth) can be readily converted to the stable cation radical $[Bu_2Ph_2Tth]^+$. The hexafluorophosphate salts of the cation radical ($[Bu_2Ph_2Tth]PF_6$) are synthesized in millimolar quantities by either chemical or constant current electrochemical oxidation; the latter method gave X-ray quality single crystals. X-ray powder diffraction studies indicate the materials from both syntheses have the same structure. The crystal structure of $[Bu_2Ph_2Tth]PF_6$ was determined and is temperature dependent. At 293 K, $[Bu_2Ph_2Tth]PF_6$ crystallizes in the *C*2/*c* space group while at 106 K it belongs to the $P2_1/n$ space group and exhibits a superlattice structure where the *c* axis is approximately double that at 293 K. Both structures consist of columnar "slipped π-stacks" of $[Bu_2Ph_2Tth]^+$ cations and channels of PF_6^- anions. At 293 K, the cations stack with a regular interplanar contact distance of 3.47 Å; at 106 K, the contact distances alternate regularly such that each cation has interplanar contact distances of 3.36(5) and 3.42(5) Å with the two neighboring cations in the π-stack. The crystal structure of Bu_2Ph_2Tth was also determined, and comparisons are made to the structure of $[Bu_2Ph_2Tth]PF_6$. Several physical techniques (UV−vis−NIR−IR absorption, spectroelectrochemistry, ESR, conductivity) were used to investigate the electronic structure of the cation radical in solution, embedded in a thin film polymer network and as a pure solid sample. The measured physical properties correlate with the crystal structures of $[Bu_2Ph_2Tth]PF_6$ and indicate that the material has a band-like electronic structure characteristic of a semiconductor.

Introduction

Studies of oligothiophene models for polythiophene suggest two likely conduction methods in oxidized polythiophene: conduction *along* a thiophene ring chain via polarons/bipolarons[1] and conduction *between* thiophene ring chains mediated through π-dimers and π-stacks.[2,3] The latter conduction method is a relatively new area of study as the π-dimer of an oligothiophene cation radical was first observed and reported in 1992.[3] Since this initial report, much work has concentrated on the study of π-dimers and π-stacks of oxidized oligothiophenes.[2−10] This work has focused on interchain electronic interactions in the solution aggregates while the structure of the interchain interactions in the solids is largely unexplored.[2−10]

Crystal structures of several neutral oligothiophenes have been reported.[11] In these structures the oligomers are typically linear, more-or-less planar, and aligned colinearly with each other, giving a layered structure. Similar structures have been proposed for the crystalline regions of poly(alkylthiophenes).[12]

* Author to whom correspondence should be addressed.

[⊗] Abstract published in *Advance ACS Abstracts,* June 1, 1997.

(1) For instance, see: (a) Heeger, A. J.; Smith, P. *Conjugated Polymers;* Bredas, J. L., Silbey, R., Eds.; Academic Publishers: Dordrecht, The Netherlands, 1991; pp 141−210 and references cited therein. (b) Furukawa, Y. *Synth. Met.* **1995**, *69*, 629. (c) Patil, A. O.; Heeger, A. J.; Wudl, F. *Chem. Rev.* **1988**, *88*, 183. (d) Heeger, A. J.; Kivelson, S.; Schrieffer, J. R.; Su, W.-P. *Rev. Mod. Phys.* **1988**, *60*, 781. (e) Chung, T.-C.; Kaufman, J. H.; Heeger, A. J.; Wudl, F. *Phys. Rev. B* **1984**, *B30*, 702.

(2) Graf, D. D.; Campbell, J. P.; Mann, K. R.; Miller L. L. *J. Am. Chem. Soc.* **1996**, *118*, 5480.

(3) (a) Hill, M. G.; Penneau, J. F.; Zinger, B.; Mann, K. R.; Miller, L. L. *Chem. Mater.* **1992**, *4*, 1106. (b) Zinger, B.; Mann, K. R.; Hill, M. G.; Miller, L. L. *Chem. Mater.* **1992**, *4*, 1113. (c) Hill, M. G.; Mann, K. R.; Miller L. L.; Penneau, J.-F. *J. Am. Chem. Soc.* **1992**, *114*, 2728.

(4) (a) Chang, A. C.; Miller, L. L. *Synth. Met.* **1987**, *22*, 71. (b) Hong, Y.; Yu, Y.; Miller, L. L. *Synth. Met.* **1995,** *74*, 133. (c) Miller, L. L.; Yu, Y.; Gunic, E.; Duan, R. *Adv. Mater.* **1995**, *7(6)*, 547. (d) Yu, Y.; Gunic, E.; Zinger, B.; Miller, L. L. *J. Am. Chem. Soc.* **1996**, *118*, 1013.

(5) (a) Bauerle, P.; Segelbacher, U.; Maier, A.; Mehring, M. *J. Am. Chem. Soc.* **1993**, *115*, 10217. (b) Bauerle, P.; Segelbacher, U.; Gaudl, K.-L.; Huttenlocher, D.; Mehring, M. *Angew. Chem., Int. Ed. Engl.* **1993**, *32(1)*, 76. (c) Segelbacher, U.; Sariciftci, N. S.; Grupp, A.; Bauerle, P.; Mehring, M. *Synth. Met.* **1993**, *55*−57, 4728.

(6) Guay, J.; Kasai, P.; Diaz, A.; Wu, R.; Tour, J. M.; Dao, L. H. *Chem. Mater.* **1992**, *4*, 1097.

(7) (a) Hotta, A.; Waragi, K. *J. Phys. Chem.* **1993**, *29*, 7427. (b) Tanaka, K.; Matsuura, Y.; Oshima, Y.; Yamabe, T.; Hotta, S. *Synth. Met.* **1994**, *66*, 295.

(8) (a) Zotti, G.; Schiavon, G.; Berlin, A.; Pagani, G. *Chem. Mater.* **1993**, *5*, 430. (b) Zotti, G.; Schiavon, G.; Berlin, A.; Pagani, G. *Chem. Mater.* **1993**, *5*, 620. (c) Zotti, G.; Berlin, G.; Pagani, G.; Schiavon, G.; Zecchin, S. *Adv. Mater.* **1994**, *6*, 231.

(9) (a) Hapiot, P.; Audebert, P.; Monnier, K.; Pernaut, J.-M.; Garcia, P. *Chem. Mater.* **1994**, *6(9)*, 1549. (b) Audebert, P.; Garcia, P.; Hapiot, P.; Monnier, K.; Pernaut, J.-M. *J. Chim. Phys.* **1995**, *92*, 827. (c) Audebert, P.; Hapiot, P.; Pernaut, J.-M.; Garcia, P. *J. Electroanal. Chem.* **1993**, *361*, 283.

(10) Nessakh, B.; Horowitz, G.; Garnier, F.; Deloffre, F.; Srivastava, P.; Yassar, A. *J. Electroanal. Chem.* **1995**, *399*, 97.

(11) (a) Miller, L. L.; Yu, Y. *J. Org. Chem.* **1995**, *60*, 6813. (b) Van Bolhuis, B.; Wynberg, H. *Synth. Met.* **1989**, *30*, 381. (c) Barbarella, G.; Zambianchi, M.; Bongini, A.; Antolini, L *Adv. Mater.* **1992**, *4(4)*, 282. (d) Effenberg, F.; Wurtlmer, F. *Angew. Chem., Int. Ed. Engl.* **1993**, *32(5)*, 719. (e) Liao, J.-H.; Benz, M.; LeGoff, E.; Kanatzidis, M. G. *Adv. Mater.* **1994**, *6(2)*, 135. (f) Gavezzotti, A.; Filippini, G. *Synth. Met.* **1991**, *40*, 257. (g) Aleman, C.; Brillas, E.; Davies, A. G.; Fajari, L.; Giro, D.; Julia, L.; Perez, J. J.; Rius, J. *J. Org. Chem.* **1993**, *58*, 3091. (h) Hotta, S.; Waragai, K. *J. Mater. Chem.* **1991**, *1(5)*, 835. (i) Paulus, E. F.; Dammel, R.; Kampf, G.; Wegener, P.; Siam, K.; Wolinski, K.; Schafer, L *Acta Crystallogr.* **1988**, *B44*, 509. (j) Visser, G. J.; Heeres, G. J.; Wolters, J.; Vos, A. *Acta. Crystallogr.* **1968**, *B24*, 467. (k) Lipka, A.; von Schnering, H. G. *Chem. Ber.* **1977**, *110*, 1377. (l) Pyrka, G. J.; Fernando, Q. *Acta. Crystallogr.* **1988**, *C44*, 562.

S0002-7863(96)04345-4 CCC: $14.00

Although oxidized oligothiophenes have been crystallized,[13] we know of no single-crystal X-ray structures other than the one in our preliminary communication: the hexafluorophosphate salt of the cation radical of 3′,4′-dibutyl-5,5″-diphenyl-terthiophene ($[Bu_2Ph_2Tth]PF_6$).[2] This structure

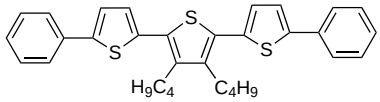

conclusively shows that an oligothiophene cation radical forms π-stacks that are similar to those of other one-dimensional organic conductors (e.g. mixed valence TTF salts[14]). These compounds typically involve π-stacks with close face-to-face contact of the molecules in the stack and have electrons delocalized intermolecularly along the stack. This structure and evidence for π-aggregates in oxidized polythiophene[15] indicate that the polaron/bipolaron conduction theory may be inadequate to describe the conductivity of oxidized oligothiophenes and polythiophene. To further investigate this problem, we designed studies to determine the structure−property relationships for $[Bu_2Ph_2Tth]PF_6$. This system was investigated by variable-temperature UV−vis−NIR−IR, ESR, single-crystal X-ray diffraction, and conductivity studies of the cation radical in solution, the solid state and also embedded in a thin-film polymer network. The crystal structure of neutral Bu_2Ph_2Tth was also obtained to determine if significant structural changes occur upon oxidation and whether these changes affect the properties of the oxidized form. In one sense then the present investigation bridges the fields of organic oligothiophene chemistry, conducting small molecule materials chemistry, and conducting polymers. Our results indicate that the conduction via π-interactions between chains is a reasonable mechanism for charge transport in this system and may be an important mechanism for charge transport in other oligothiophene and polythiophene systems.

Experimental Section

General Considerations. Solvents for UV−vis−NIR−IR absorption/emission, electrochemical and spectroelectrochemical studies were dried by distillation (under N_2) of dichloromethane from P_2O_5 and acetonitrile from CaH_2. 3′,4′-Dibutyl-2,5″-diphenyl-2,2′:5′,2″-terthiophene was synthesized as reported earlier.[2] Poly(methylmethacrylate) (PMMA) and hexafluoro-2-propanol were purchased from Aldrich Chemical Co. and used as received.

X-ray powder diffraction patterns were collected on a Siemens powder diffractometer at room temperature with Cu Kα radiation (1.540 562 Å) generated by a rotating anode operating at 45 kV and 40 mA. All conductivity measurements were obtained by the four-probe colinear conductivity method. Iodine doping of Bu_2Ph_2Tth was carried out by placing a sample of Bu_2Ph_2Tth in an I_2 chamber for 20 h. During this time, the sample color changed from yellow to purple, which is characteristic of oxidation of Bu_2Ph_2Tth to $[Bu_2Ph_2Tth]^+$.

Electrochemical Measurements. Electrochemical experiments were performed with a BAS 100 electrochemical analyzer. Cyclic voltammetry (CV) and chronocoulometry (CC) experiments were performed at room temperature (23−24 °C) with a normal three-electrode configuration consisting of a highly polished glassy-carbon working electrode ($A = 0.07$ cm^2), a Pt auxiliary electrode, and a Ag/AgCl reference electrode containing 1.0 M KCl. The 5-mL working compartment was separated from the reference compartment by a modified Luggin capillary. All three compartments were filled with a 0.1 M solution of supporting electrolyte. Tetrabutylammonium hexafluorophosphate ($TBA^+PF_6^-$) was purchased from Southwestern Analytical Chemicals and stored in vacuum prior to use. The electrolyte solution was passed down a column of activated alumina prior to the electrochemical experiments. The working compartment of the cell was bubbled with solvent-saturated argon to deaerate the solution. The working solutions were prepared by recording the background cyclic voltammograms of the electrolyte solution prior to addition of the solid sample.

Potentials are reported versus aqueous Ag/AgCl and are not corrected for the junction potential. The $E^{o\prime}$ value for the ferrocenium/ferrocene couple was determined for a solution with a concentrations similar to those used in the study of Bu_2Ph_2Tth to allow correlation of the E^o values to past and future studies. For a 0.54 mM dichloromethane solution of ferrocene, the oxidation and reduction waves occurred at +513 and +402 mV, respectively ($E^{o\prime} = +458$ mV). The diffusion coefficient for this ferrocene sample was calculated to be 2.93×10^{-6} cm^2/s ($n = 1$) from chronocoulometry studies ($E_{appl} = 0$ to 600 mV) and a linear Anson plot of Q vs $t^{1/2}$.

UV−vis Spectroelectrochemical Studies. Spectroelectrochemical studies were performed in a flow-through thin-layer cell previously described.[16] Spectra were recorded with a Tracor Northern TN-6500 rapid-scan diode-array apparatus with a Xe arc lamp as the light source. Electrolyses were controlled by a BAS-100 bulk electrolysis program. The solutions used for these studies were prepared as for the electrochemical studies and then transferred to the thin-layer cell via glass syringe. A CV of the sample in the thin-layer cell was used to determine the applied potential needed for the bulk electrolysis. Spectra were recorded at periodic intervals during the electrolysis.

UV−vis−NIR−IR Studies. UV−vis−NIR spectra (200−2400 nm) were recorded with a Cary-17 spectrometer. In certain cases, the NIR−IR spectra (800−2850 nm) were also recorded with a Nicolet Magna-IR spectrometer. Solutions of Bu_2Ph_2Tth for UV−vis studies were prepared by dissolving the compound in an appropriate volume of solvent to give the highest measured absorbance of 1.0−1.2 in the 1 cm path length quartz cell. Solutions of $[Bu_2Ph_2Tth]^+$ for UV−vis−NIR−IR studies were prepared by charging a 50-mL Schlenk flask with a small amount (0.1−1 mg) of the desired compound. The flask was purged three times, an appropriate amount of freshly distilled solvent was added, and the mixture was stirred to ensure complete dissolution. The sample cells (1 cm and 0.1-cm quartz cells) were dried in an oven and degassed with Ar as they cooled. The solutions were then transferred to the quartz cells via cannulation with *Teflon tubing*. The absorbance of the solution was then adjusted by dilution to give absorbances of 1.1 or less. For Bu_2Ph_2Tth and $[Bu_2Ph_2Tth]^+$, extinction coefficients were calculated from the experimentally determined absorbances and concentrations with Beer's law.

Solid state samples for UV−vis−NIR−IR studies were prepared as ground films on CaF_2 plates by placing a small amount of the solid compound between two plates and grinding until a uniform film was obtained. The spectra of the films typically had a background absorbance of 0.1−0.4 (due to back-reflection by the reflective film). Spectral shape and peak positions were similar for all films prepared by this method.

Variable-temperature solution and solid state UV−vis−NIR spectra were recorded in a locally constructed quartz dewar designed to fit the Cary-17 sample chamber. The temperature was controlled by adjusting the flow of a liquid nitrogen cooled stream of nitrogen gas into the dewar. The temperature was monitored by a thermocouple in contact with the cell holder and remained within ±3 °C of the desired value. Samples were allowed to equilibrate at the desired temperature for at least 5 min before the spectra were recorded.

ESR Studies. ESR spectra were recorded with an X-Band IBM-Bruker ESP-300 spectrometer equipped with a variable-temperature cavity. During the course of an experiment, the temperature remained

(12) Prosa, T. J.; Winokur, M. J.; Moulton, J.; Smith, P.; Heeger, A. J. *Synth Met.* **1993**, *55*, 370.

(13) Matsuura, Y.; Oshima, Y.; Misaki, Y.; Fujiwara, H.; Tanaka, K.; Yamabe, T.; Hotta, S. *Synth. Met.* **1996**, *82*, 155.

(14) See, for example: (a) Baumgarten M.; Mullen, K. *Top. Curr. Chem.* **1993**, *165*, 3−92 and references cited therein. (b) Miller, J. S., Ed.; *Extended Linear Chain Compounds*, Plenum Press: New York, 1982; Vol. 2, and references cited therein.

(15) (a) Cornil, J.; Beljonne, D.; Bredas, J. L *J. Chem. Phys.* **1995**, *103-(2)*, 834. (b) Zotti, G.; Berlin, A.; Pagani, G.; Schiavon, G.; Zecchin, S. *Adv. Mater*. **1994**, *6*, 231. (c) Hong, Y. L.; Miller, L. L. *Chem Mater*. **1995**, *7*, 1999.

(16) Bullock, J. B.; Mann, K. R. *Inorg. Chem.* **1989**, *28*, 4006.

Table 1. Crystal Data and Structure Refinement[a] for Bu_2Ph_2Tth and $[Bu_2Ph_2Tth]PF_6$

compd	Bu_2Ph_2Tth	$[Bu_2Ph_2Tth]PF_6$
formula	$C_{32}H_{32}S_3$	$C_{32}H_{32}F_6PS_3$
formula wt	512.76	657.73
temp, K	297(2)	106(2)
wavelength, Å	0.71073	0.71073
crystal system	orthorhombic	monoclinic
space group	$Pca2_1$	$P2_1/n$ (no. 14)
a, Å	15.3613(1)	34.5206(1)
b, Å	30.6753(3)	20.1750(2)
c, Å	5.8925(1)	8.6590(1)
β, deg	90	92.858(1)
vol, Å^3	2776.62(6)	6023.09(9)
Z	4	8
density (calcd), mg/m^3	1.227	1.451
abs coeff, mm^{-1}	0.286	0.359
abs corr	none	Sadabs
F(000)	1088	2728
crystal size, mm	0.52 × 0.12 × 0.08	0.5 × 0.15 × 0.12
crystal habit/color	needle/orange	needle/green
θ range for data collection, deg	0.66−24.12	1.17−25.02°
index ranges	$-14 < h < 17$	$-40 < h < 40$,
	$-33 < k < 35$	$-18 < k < 23$
	$-6 < l < 6$	$-10 < l < 9$
no. of reflcns collected	12774	27878
no. of independent reflcns	4268 ($R_{int} = 0.0930$)	10420 ($R_{int} = 0.0572$)
data/restraints/parameters	4267/13/348	10420/123/ 842
goodness-of-fit on F^2	1.104	1.054
final R indices [$I > 2\sigma(I)$]	$R1 = 0.0835$, $wR2 = 0.1958$	$R1 = 0.0776$, $wR2 = 0.1818$
R indices (all data)	$R1 = 0.1004$, $wR2 = 0.2146$	$R1 = 0.1410$, $wR2 = 0.2124$
largest diff peak and hole, e Å^{-3}	0.318 and −0.326	1.082 and −0.369

[a] The refinement method for both structures was full-matrix least squares on F^2. For $[Bu_2Ph_2Tth]PF_6$, the weighting scheme was $w = [s^2(F_o^2) + (AP)^2 + (BP)]^{-1}$, where $P = (F_o^2 + 2F_c^2)/3$, $A = 0.0864$, and $B = 8.9397$.

within ±2 °C of the desired value. The intensity of each spectrum was determined by double integration, and each spectrum was integrated twice to ensure reproducible values. The magnetic field was calibrated with either a dichloromethane solution ($g = 2.0012$) or solid sample ($g = 2.0040$) of 2,2-diphenyl-1-picrylhydrazyl hydrate, DPPH (Aldrich).

For solution ESR studies, quartz ESR tubes (5-mm diameter) were charged with a small amount of the oxidized compound and sealed with a septum and parafilm while in a N_2-filled glovebox. The samples were removed from the glovebox and dry solvent was added followed by careful shaking to ensure the dissolution of all the material. Direct contact of the solution with the septum was avoided as this typically results in some loss of $[Bu_2Ph_2Tth]^+$ via decomposition and/or reduction (as evidenced by the change in the solution color from blue to green to yellow over a few minutes). Solid state ESR samples were prepared in air by thoroughly grinding the solids and placing the solid in quartz ESR tubes (5 mm).

Spin counting studies for solid state samples of DPPH and $[Bu_2Ph_2Tth]^+$ were performed by adding a known amount of each compound into the ESR tube. Three samples were prepared for each compound with varying amounts of the material (5−20 mg). The sample tubes were placed in the spectrometer, taking care to ensure the samples were placed in exactly the same position for each experiment. A spectrum of each sample was recorded with the same acquisition parameters, and each spectrum was doubly integrated at least twice to ensure reproducible integration values. The ESR spectral intensity per mole of unpaired electrons in the DPPH standard was determined and then used to calculate the number of moles of unpaired electrons per mole for the $[Bu_2Ph_2Tth]^+$ samples.

Preparation of Bu_2Ph_2Tth/PMMA and $[Bu_2Ph_2Tth]PF_6$/PMMA Films. Thin films of Bu_2Ph_2Tth imbedded in a PMMA network were cast on glass slides by solvent evaporation (in air at room temperature and atmospheric pressure) of a solution of the appropriate amounts of PMMA and Bu_2Ph_2Tth in 1 mL of CH_2Cl_2. Thin films of $[Bu_2Ph_2Tth]PF_6$ imbedded in a PMMA network were cast on glass slides as for neutral Bu_2Ph_2Tth. The casting solution was prepared by dissolving the appropriate amounts of PMMA and Bu_2Ph_2Tth (not completely soluble) in 1 mL of hexafluoro-2-propanol. A weighted amount of $NOPF_6$ (usually 20% excess) was added to the solution upon which the solution quickly turns dark blue and all the Bu_2Ph_2Tth dissolved. The solution was stirred for 5 min to ensure full oxidation of Bu_2Ph_2Tth. Films of half-oxidized $[Bu_2Ph_2Tth]^+$/PMMA were made as for fully oxidized films of $[Bu_2Ph_2Tth]^+$/PMMA except that only half an equivalent of $NOPF_6$ was used.

Single Crystal X-ray Data Collection for Bu_2Ph_2Tth. Crystals of Bu_2Ph_2Tth were grown by slow evaporation of a 4:1 (v:v) methanol−dichloromethane solution of the compound. A single crystal of the compound was attached to a glass fiber and mounted on the Siemens SMART system for data collection at 297(2) K. An initial set of cell constants was calculated from reflections harvested from three sets of 20−30 frames. These initial sets of frames are oriented such that orthogonal wedges of reciprocal space were surveyed. This produced orientation matrices determined from 50−300 reflections. Final cell constants are calculated from a set that does not exceed a number equal to 8192 of strong reflections from the actual data collection. The data were collected by the hemisphere collection method where a randomly oriented region of reciprocal space is surveyed to the extent of 1.3 hemispheres to a resolution of 0.84 Å. Three major swaths of frames are collected with 0.30° steps in ω. Further details of the data collection are given in Table 1, and selected experimental data are given in Table 4. All experimental data are provided as Supporting Information.

The space group $Pca2_1$ was determined on the basis of systematic absences and intensity statistics.[17] A successful direct-methods solution was calculated which provided most non-hydrogen atoms from the E-map. Several full-matrix least squares/difference Fourier cycles were performed which located the remainder of the non-hydrogen atoms. All non-hydrogen atoms were refined with anisotropic displacement parameters unless stated otherwise. All hydrogen atoms were placed in ideal positions and refined as riding atoms with individual (or group if appropriate) isotropic displacement parameters. A total of 12 SADI distance restraints were applied to C(12)−C(16) and C(18)−C(21) to keep the bond lengths equal and minimize the effects of thermal motion.

Single-Crystal X-ray Data Collection for $[Bu_2Ph_2Tth]PF_6$ at 106 K. The unit cell constants were determined at eight temperatures between 297 and 106 K to determine if these values reflected a structural change at lower temperatures. The mounted crystal from the 293 K study[2] of the compound was encased in epoxy, transferred to the

(17) The programs used for X-ray analysis were part of SHELXTL-Plus V5.0 by Siemens Industrial Automation, Inc., Madison, WI.

Table 2. Variable-Temperature Unit Cell Experiment[a] for $[Bu_2Ph_2Tth]PF_6$

T (°C)	a (Å)	b (Å)	c (Å)	β (deg)	V (Å^3)	no. of refs	$\lvert\vec{k}_{[101]}\rvert$ (Å)[b]
+24(2)	8.478(3)	20.616(7)	18.029(6)	91.00(7)	3151(2)	40	19.79
−34(2)	8.613(3)	20.487(6)	35.126(9)	92.01(3)	6194(3)	55	35.87
−52(2)	8.627(2)	20.449(6)	34.984(9)	92.212(4)	6167(4)	50	35.71
−75(2)	8.640(2)	20.376(6)	34.801(8)	92.44(3)	6121(3)	65	35.50
−100(2)	8.652(2)	20.308(5)	34.681(8)	92.62(3)	6087(3)	67	35.36
−125(2)	8.653(2)	20.251(6)	34.589(8)	92.80(2)	6053(3)	63	35.24
−149(2)	8.651(2)	20.185(5)	34.510(8)	92.95(3)	6018(3)	82	35.14
−167(2)	8.650(2)	20.150(5)	34.479(7)	93.03(2)	6001(3)	89	35.10

[a] The unit cell is centered at 24 °C but is primitive at all other temperatures studied. [b] $\lvert\vec{k}_{[101]}\rvert = [a^2 + c^2 + 2ac\cos(\beta)]^{1/2}$.

goniometer of a Siemens SMART CCD System, and cooled to the desired temperature with a Siemens LT-2 low-temperature device. Crystal quality and centering was confirmed by taking a 60 s rotation frame. A search was performed by taking a series of frames in three orthogonally related regions of reciprocal space. Each region investigated comprised twenty 10-s frames, 0.3° apart in ω. These were harvested to yield a total of 40−89 reflections with intensities greater than 10σ. An initial unit cell was obtained, and checked for centering and higher symmetry. The 297 K data showed the presence of C-centering while the low-temperature cells were all primitive. The initial cell constants were refined, and an initial orientation matrix was found. The unit cells obtained are listed in Table 2. All measurements were taken on the same crystal.

Intensity data was collected at 106 K by examining a randomly oriented region of reciprocal space in three segments; the frames collected in a given segment were 0.3° apart in ω. The highest resolution data collected was 0.87 Å. The total shutter open time for each double-correlated frame was 60 s; two 30 s frames were collected, and the data summed, doubling the dynamic range of the detector. The default gain of the detector signal was 4×, which was automatically dropped to 1× when the detector range was exceeded. Final cell constants were determined during integration of the data, using 8192 intense, well-centered reflections. Further details of the data collection are given in Table 1, and selected experimental data are given in Table 4. All experimental data are provided as Supporting Information.

The variable-temperature results showed that the compound formed a superlattice at lower temperatures with approximate doubling of the c axis between 297 and 106 K. Careful examination of the intensity data during processing (XPREP[17]) ruled out the possibility of centering, or of a mistaken axis doubling. Successful solution and refinement of the structure confirms the choice of cell.

The space group at 106 K was determined to be $P2_1/n$ on the basis of systematic extinctions and intensity statistics.[17] The structure was solved by using the direct methods program **xs**.[17] Hydrogens were placed in calculated positions and refined with a riding model with B values 20% larger than those on the attached carbon atoms. The asymmetric unit contains two complete molecules, related by a pseudoinversion center. The two independent molecules were constrained to have corresponding bond distances equal with use of the SAME[17] instruction. One *n*-butyl group on each molecule is disordered (70%/30%) over two positions. The disordered atoms were refined anisotropically with the constraint ISOR[17] to keep the ellipsoids approximately spherical, and with the appropriate occupancy. Full anisotropic refinement of all non-hydrogen atoms was performed by using full-matrix least squares on F^2 with the program **xl**,[17] yielding a final $R_1 = 0.0776$ (4σ, based on F^2). An absorption correction was applied to the data prior to solution and refinement by with the program SADABS **(SAD)**.[17] The final difference map was essentially flat, with maximum and minimum peaks corresponding to 1.082 and −0.369 e$^-$/Å^3. Scattering factors and anomalous scattering terms were taken from the usual sources,[18] and the effects of anomalous dispersion were included for the non-hydrogen atoms.

Results

Electrochemical Properties. A cyclic voltammogram of a 0.55 mM solution of Bu_2Ph_2Tth in 0.1 M $TBAPF_6$/dichloromethane exhibits two reversible one-electron processes with $E^o_{1+/0} = 0.89$ V and $E^o_{2+/1+} = 1.29$ V. The peak separation is 84 mV for both processes, and the $i_{p,c}/i_{p,a}$ ratio for the first and second processes is 0.99 and 1.05, respectively. The $i_{p,c}/i_{p,a}$ values for the second oxidation are less reliable due to a current "spike" in the coupled reductive process that is indicative of insolubility of one or more of the charged species at the electrode. Repeated scanning from 0.0 to +1.8 V yielded identical CVs, which indicates that no polymerization or decomposition occurs for the oxidized forms. Chronocoulometry experiments were used to calculate the diffusion coefficient from a linear Anson plot (Q vs $t^{1/2}$). For the first oxidative process (E = 500 to 1100 mV), the calculated diffusion coefficient in dichloromethane for $n = 1$ is 2.47×10^{-5} cm^2/s. For experiments covering the first and second oxidative processes (E = 500 to 1500 mV), the calculated diffusion coefficient for $n = 2$ is 2.32×10^{-5} cm^2/s. The similarity of these diffusion coefficients to one measured for ferrocene under the same conditions (2.5×10^{-5} cm^2/s) indicates each oxidation is a one-electron process that sequentially leads to the cation radical and dication forms.

UV−vis Absorption/Emission Studies of Neutral Bu_2Ph_2Tth. The electronic spectrum of neutral Bu_2Ph_2Tth in dichloromethane exhibits two bands: a moderately intense band at 264 nm ($\epsilon = 1.6 \times 10^4$ M^{-1} cm^{-1}) and an intense band at 384 nm ($\epsilon = 3.1 \times 10^4$ M^{-1} cm^{-1}) (Supporting Information). The low-energy band is attributed to a $\pi-\pi^*$ transition of the conjugated thiophene system[19] and the high-energy band is tentatively attributed to a $\pi-\pi^*$ local excitation of the heteronucleus.[20] The low-energy band is asymmetric and exhibits a distinct high-energy tail. Excitation of the $\pi-\pi^*$ band of the compound (λ_{ex} = 390 nm) leads to an intense structured emission which nearly mirrors the high-energy tail of the absorption spectrum (see Supporting Information). The emission has three distinct λ_{max} values at 468, 498, and 540 nm with relative intensities of 100:80:33, respectively.

UV−vis Spectroelectrochemical Studies. Spectroelectrochemical oxidation of Bu_2Ph_2Tth in 0.1 M $TBAPF_6/CH_2Cl_2$ leads to significant changes in the UV−vis spectral region (300 to ca. 830 nm). One-electron oxidation causes the 384-nm band to disappear as a new band and two shoulders grow in isosbestically at 655, 530, and 585 nm, respectively (Figure 1A). The oxidation is chemically reversible as reduction at 0.0 V reproduces the starting spectrum with >95% of the original intensity. Spectroelectrochemical oxidation of Bu_2Ph_2Tth in acetonitrile leads to similar behavior: the 380-nm band disappears as a new band and two shoulders grow in isosbestically at 638, 520, and 573 nm, respectively.

The removal of the second electron caused the 654-nm band (and shoulders) to disappear as two large new bands grow in at 735 and 805 nm with smaller bands growing in at 450 and 525

(18) Wilson, A. J. C., Ed. *International Tables for Crystallography;* Kluwer Academic Publishers, Dordrecht, 1995; Vol. C.

(19) Murrell, J. N. *J. Chem. Soc.* **1956**, 3779.

(20) Curtis, R. F.; Phillips, G. T. *Tetrahedron* **1967**, *23*, 4419.

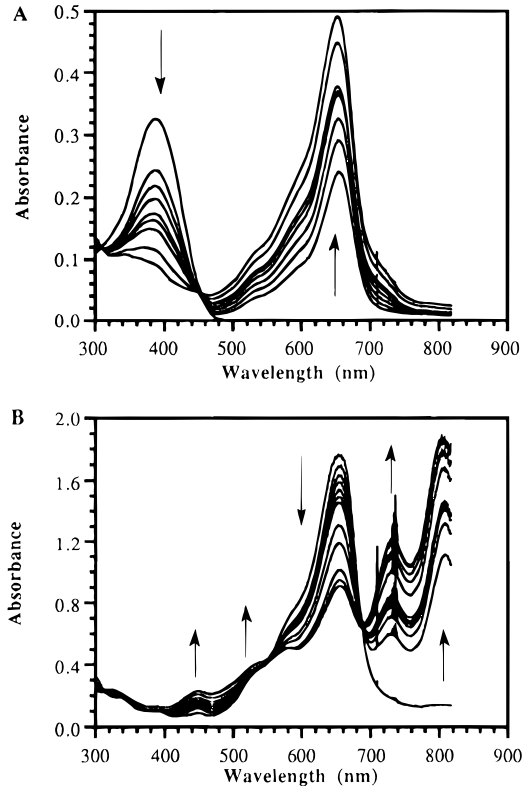

Figure 1. UV−vis spectra recorded during the spectroelectrochemical oxidation of Bu_2Ph_2Tth in 0.1 M $TBA^+PF_6^-/CH_2Cl_2$ ($[Bu_2Ph_2Tth]_{initial}$ = 0.11 mM; T = 22 °C). Spectra were recorded approximately every 10 s (A) during the passage of 1 e^-/molecule at $E_{applied}$ = 0.75 V and (B) during the passage of a second 1 e^-/molecule at $E_{applied}$ = 1.4 V (vs the pseudo Pt reference of the thin-layer cell). Sharp features at 700−710 nm are an instrumental artifact.

Table 3. UV−vis−NIR−IR Spectra for $[Bu_2Ph_2Tth]PF_6$ in Solution and the Solid State[a]

	solvent	λ_{max} (nm)
$[Bu_2Ph_2Tth]^+$	CH_2Cl_2	1106,[b] 980 (sh), 654,[b] 530 (sh), 585 (sh)
$[Bu_2Ph_2Tth]^+$	CH_3CN	1075, 950 (sh), 638, 520 (sh), 573 (sh)
$[Bu_2Ph_2Tth]_2^{2+}$	CH_2Cl_2	1275, 1012, 590[c]
$[Bu_2Ph_2Tth]_2^{2+}$	CH_3CN	1325, 995, 580[c]
$[Bu_2Ph_2Tth]PF_6$	solid state	625,1075, 1500−2600

[a] Compounds are the PF_6^- salt. Spectra are identical for chemically oxidized or electrocrystallized samples. [b] The molar absorptivity was determined for this sample to be $\epsilon = 6.0 \times 10^4$ M^{-1} cm^{-1} at 654 nm and $\epsilon = 6.0 \times 10^4$ M^{-1} cm^{-1} at 1106 nm. [c] The spectra for the π-dimers were determined at low temperature as discussed in the text.

nm (Figure 1B). The oxidation did not go to completion, most likely due to coverage of the electrode by the $[Bu_2Ph_2Tth]^+$ and/or $[Bu_2Ph_2Tth]_2^{2+}$ dimer species which are expected to slow the rate of oxidation of the bulk solution (as is observed during the electrocrystallization process). These spectral changes are consistent with the formation of $[Bu_2Ph_2Tth]^{2+}$ as the band positions and shapes are in good agreement with those observed for the dications of other oligothiophenes.[3a,b,5,6,7a,21] The second oxidation process is chemically reversible as bulk reduction at 0.0 V regenerates the spectrum of neutral Bu_2Ph_2Tth with >95% of the original intensity.

UV−vis Absorption Studies of Oxidized Bu_2Ph_2Tth. The room temperature dichloromethane solution spectrum of $[Bu_2Ph_2Tth]PF_6$ exhibits two main bands (Table 3, Figure 2) and several small shoulders. The spectrum of $[Bu_2Ph_2Tth]PF_6$ in acetonitrile is similar but blue shifted (Table 3). Cooling a dichloromethane solution (1.9×10^{-4} M) of $[Bu_2Ph_2Tth]^+$ causes the intensity of the bands at 1106 and 654 nm to first increase slightly until at or below 260 K, then their intensities decrease as new bands grow in isosbestically at 1275, 1012, and 590 nm (Figure 3). The spectral changes are completely reversed by warming the solution back to room temperature. Similar variable-temperature behavior is observed for acetonitrile solutions of $[Bu_2Ph_2Tth]PF_6$: below 273 K, the bands at 1075 and 638 nm decrease as three new bands grow in isosbestically at 1325, 995, and 580 nm. These spectral changes are reversed by warming the solution to room temperature. The three new bands in the low-temperature spectra in both solvents most likely correspond to the π-dimer of two cation radicals as has been reported for π-dimers of other oligothiophene cation radicals.[3−5] At room temperature, there is no direct evidence for the presence of these π-dimers. For example, dichloromethane and acetonitrile solutions of $[Bu_2Ph_2Tth]^+$ were prepared with concentrations which varied by two orders of magnitude (10^{-4}−10^{-6} M). The spectra of the dilute and concentrated solutions are similar, indicating that π-dimerization is unfavorable at room temperature at these concentrations.

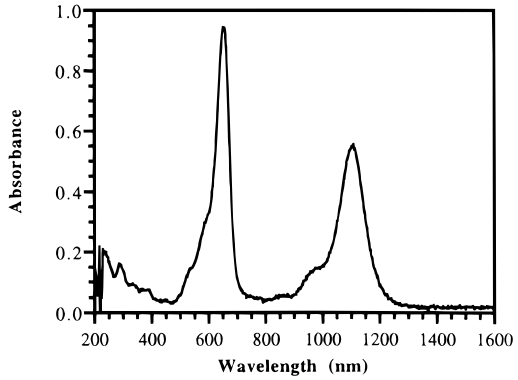

Figure 2. Room temperature UV−vis−NIR absorption spectrum of $[Bu_2Ph_2Tth]PF_6$ in dichloromethane.

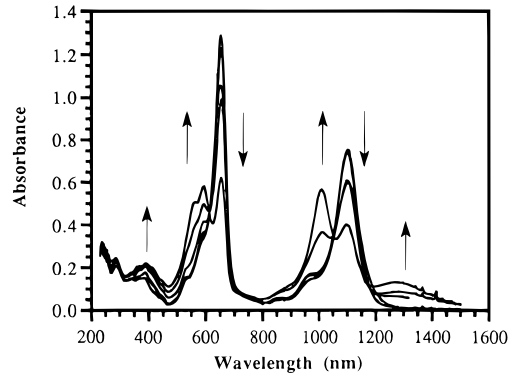

Figure 3. UV−vis−NIR absorption spectrum of $[Bu_2Ph_2Tth]PF_6$ in dichloromethane recorded as the temperature was lowered from 295 K to 270, 250, 230, 215, and finally 205 K. The absorbance of the bands at 654 and 1106 nm first increases slightly upon cooling until below 250 K where it decreases as the π-dimer bands grow in isosbestically. All changes are reversible.

The equilibrium constant (K_{eq}) for the π-dimerization was determined from the variable-temperature studies of the cation radical solutions. The relative concentrations of the monomeric and dimeric species at different temperatures has been approximated on the basis of the change in the absorbance for the monomeric cation radical.[22] This approximation is necessary as the extinction coefficient for the π-dimer cannot be reliably determined at any given temperature studied. The equilibrium

(21) Bauerle, P. *Adv. Mater.* **1992**, *4*, 102.

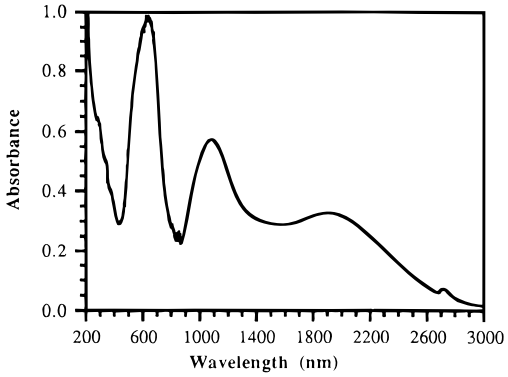

Figure 4. Room temperature UV−vis−NIR−IR absorption spectrum of $[Bu_2Ph_2Tth]PF_6$ as a ground film on CaF_2 plates.

constant at 295 K is calculated to be $3(5) \times 10^{-4}$ in dichloromethane and 0.6(5) in acetonitrile. The large uncertainties in the values of K_{eq} are due to the temperature dependence of the measured absorbance of the monomeric species and the large overlap of the bands for the monomeric and dimeric species. Although these values have a large range, the magnitude of the values is very reasonable compared to the K_{eq} values determined for other oligothiophene cation radicals.[3,4d,5a] For example, the cation radical of 5,5″-dimethyl-2,2′:5′,2″-terthiophene (Me_2Tth) forms π-dimers at room temperature (at 10^{-4} M) and has a K_{eq} of about 154 in acetonitrile.[3c] The lack of π-dimerization for $[Bu_2Ph_2Tth]^+$ under similar conditions is consistent with the K_{eq} being much smaller for $[Bu_2Ph_2Tth]^+$ than for $[Me_2Tth]^+$.

The electronic spectra of solid-state samples of $[Bu_2Ph_2Tth]PF_6$ from electrocrystallization and chemical oxidation are nearly identical. Each spectrum exhibits two main bands similar in position to that of the monomeric and dimeric cation radical in solution, but the bands in the solid-state spectrum are much broader (Figure 4). In addition, there is a distinct, very broad NIR band that extends into the IR region (Figure 4). This low-energy band is typically observed for π-stacked molecules and is attributed to an intra-stack charge transfer (i.e. the optical conduction band).[4b,c] Cooling the film on the CaF_2 plate causes some sharpening of the lower energy side of the vis and NIR bands while the center of the broad NIR−IR charge transfer band blue shifts from 1920 nm at 290 K to about 1780 nm at 190 K.

ESR Studies. Dichloromethane solutions of $[Bu_2Ph_2Tth]^+$ exhibit a highly structured room temperature ESR spectrum centered at $g = 2.0014$. The signal exhibits a basic 16-line spectrum where each "line" has one or more shoulders, which leads to an overall broadening of the spectrum (Figure 5). Lowering the temperature leads to significant changes in the structure and intensity of the ESR signal (Figure 5). The g value increases as the temperature is lowered until at or below about 260 K the g value becomes constant at 2.0025. Furthermore, the ESR signal exhibits at least 30 distinct lines below 260 K. At low temperature it appears that the shoulders of the room temperature spectrum become distinct lines. The complex

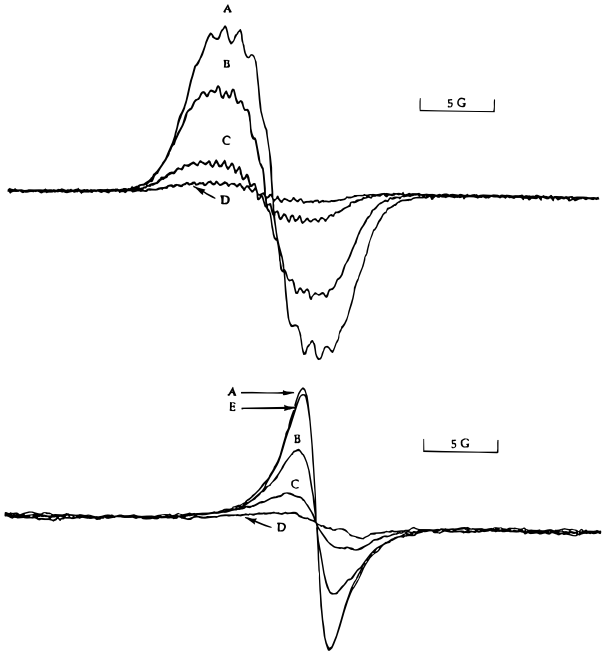

Figure 5. ESR spectra of $[Bu_2Ph_2Tth]PF_6$: (top) as a dichloromethane solution at (A) 290 ($g = 2.0014$), (B) 260, (C), 230, and (D) 200 K ($g = 2.0025$); (bottom) as a ground sample of electrocrystallized $[Bu_2Ph_2Tth]PF_6$ at (A) 290, (B) 280, (C) 235, and (D) 185 K and (E) warmed to 290 K after the cooling process.

spectra most likely result from the presence of at least two rotational isomers, as has been observed for other oligothiophenes.[3b,23] Attempts to simulate the spectra with one or more isomers were unsuccessful.

The intensity of the ESR signal for $[Bu_2Ph_2Tth]^+$ in solution is also temperature dependent. Cooling a $[Bu_2Ph_2Tth]^+$ dichloromethane solution (10^{-4} M) to 200 K decreases the signal intensity to only 5% that at 290 K. Warming the sample back to 290 K causes the ESR spectrum to return to its original intensity and shape. For comparison, cooling a dichloromethane solution of DPPH from 290 K to 190 K did not change the intensity of the spectrum. The temperature dependence of the ESR signal for $[Bu_2Ph_2Tth]^+$ is attributed to the reversible π-dimerization of the cation radicals to give a diamagnetic dication.[3,4b,5b,c]

Ground solid samples of $[Bu_2Ph_2Tth]PF_6$ exhibit relatively sharp, unstructured ESR signals centered at $g = 2.0025$ (Figure 5). The intensity of the ESR signal of the solid samples is also temperature dependent (Figure 5). Relative to the signal intensity at 290 K for a ground sample of chemically produced $[Bu_2Ph_2Tth]PF_6$, the intensity is 67%, 33%, and 13% at 280, 235, and 185 K, respectively. Upon warming back to 290 K, the signal returns to its original intensity. Relative to the signal intensity at 290 K for a ground sample of electrocrystallized $[Bu_2Ph_2Tth]PF_6$, the intensity is 52 and 33% at 236 and 190 K, respectively. Upon warming back to 290 K, the signal returns to its original intensity. For comparison, cooling a solid sample of DPPH from 290 K to 190 K did not change the intensity of the spectrum.

ESR spin count experiments were also performed to determine how many unpaired electrons are responsible for the ESR signal from the solid samples. The number of unpaired electrons per mole of $[Bu_2Ph_2Tth]PF_6$ was calculated to be 0.16 and 0.14 at room temperature for the chemically and electrochemically produced solids, respectively. These results indicate there are

(22) The change in the absorbance for the monomeric cation radical is directly related to the change in concentration of the monomeric species by $\Delta C_m = C_m^o - C_m = (A^o - A)/(\epsilon b)$ {C_m, A = concentration and absorbance of monomeric species at temperature T; C_m^o, A^o = initial concentration and absorbance of monomeric species; ϵ = extinction coefficient; b = cell path length}. The concentration of the dimer (C_d) is assumed to simply be half of the change in the concentration of the monomeric species ($C_d = {}^1/_2(C_m^o - C_m)$. Based on this, the equilibrium constant was calculated at 260, 210, and 200 K as $K_{eq} = [C_d]/[C_m]^2 = {}^1/_2(\epsilon b)(A^o - A)/A^2$. The equilibrium constant at 295 K was then calculated from a plot of $-\ln(K_{eq})$ vs $1/T$.

(23) Alberti, A.; Favaretto, L.; Seconi, G. *J. Chem. Soc., Perkin Trans.* **1990**, *2*, 931.

only about 15 unpaired electrons per 100 $[Bu_2Ph_2Tth]^+$ units in the samples.

Conductivity Measurements. Pressed pellets of $[Bu_2Ph_2Tth]PF_6$ were subjected to conductivity measurements by a four-probe method. At room temperature, the conductivity of pressed pellets of the electrocrystallized and chemically oxidized forms was found to be $2-3 \times 10^{-3}$ S/cm. Cooling the sample to −78 °C lowered the conductivity to only 3×10^{-5} S/cm for both samples. The drop in the conductivity is reversed by warming the sample back to room temperature. The conductivity of a sample of Bu_2Ph_2Tth exposed to I_2 vapor for 20 h was measured to be 1.5×10^{-2} S/cm. The conductivity of the samples at all temperatures is electronic and stable, and no polarization was observed.

X-ray Powder Diffraction Studies. The powder X-ray diffraction pattern for electrochemically and chemically synthesized samples of $[Bu_2Ph_2Tth]PF_6$ was recorded. Each sample gives an identical powder diffraction pattern[24] with several intense lines at $2\theta < 30°$. These samples appear to be highly crystalline as the diffraction lines are sharp and there are no broad reflections due to amorphous components. The 12 best-resolved lines of the diffraction pattern were indexed[25] on the basis of the known structure of $[Bu_2Ph_2Tth]PF_6$, and the results are given as Supporting Information. The shoulders and weak lines in the 2θ region of 15−30° were not indexed due to the large uncertainty in their experimental values. The good agreement of the experimental and calculated lines for the sample indicates that the bulk sample has the same structure as found for the crystals selected for X-ray crystallography studies. Furthermore, the small number of lines observed in the powder diffraction is consistent with a unit cell of centered symmetry as this leads to a large number of systematic absences in the diffraction lines.[25]

The X-ray powder diffraction pattern[24] of neutral Bu_2Ph_2Tth exhibits several intense lines at $2\theta < 25°$ and several weaker lines at $2\theta > 25°$. The 16 best-resolved lines were indexed on the basis of the known crystal structure of this compound.[25] The several shoulders and weak lines in the region of $2\theta \geq 25°$ were not indexed due to poor signal to noise and the large number of possible Miller indexes which correspond to these high angle reflections. The experimental and calculated *d* spacings for these lines correlate well and indicate that the bulk sample is the same as the single crystal selected for X-ray crystallography. The diffraction pattern also indicates that the bulk sample is highly crystalline as the diffraction lines are sharp and there are no broad reflections due to amorphous components.

A powder diffraction pattern[24] was also collected for a sample of Bu_2Ph_2Tth doped with I_2 for 20 h. This sample exhibits lines at 6.45° (13.6925 Å), 6.95° (12.7085 Å), 10.80° (8.1852 Å), 18.55° (4.779 Å), and 26.1° (3.4114 Å). Unfortunately, the small number of diffraction lines, weak intensity, and poor signal-to-noise ratio did not allow an accurate determination of the unit cell for the sample. The diffraction pattern of this sample does show several similarities and differences compared to that of the Bu_2Ph_2Tth and $[Bu_2Ph_2Tth]PF_6$ patterns, but as the counterion is different, it is hard to make any structural statements concerning the sample. It is likely that the I_2-doped form of Bu_2Ph_2Tth has a different structure from either Bu_2Ph_2Tth or $[Bu_2Ph_2Tth]PF_6$.

Films of Bu_2Ph_2Tth and $[Bu_2Ph_2Tth]PF_6$ Embedded in a PMMA Network. Fully oxidized films of Bu_2Ph_2Tth with 5, 10, 15, and 20 wt % loading in poly(methylmethacrylate) (PMMA) films were prepared. Very stable purple films could be produced by casting from a hexafluoro-2-propanol solution while films cast from CH_2Cl_2 were unstable with respect to reversion to the neutral form (even if a large excess (3-fold) of $NOPF_6$ was used). All films studied were therefore cast from hexafluoro-2-propanol solutions.

The vis−NIR absorption spectrum of pure $[Bu_2Ph_2Tth]^+$ films show bands at 600, 1100, and 2000 nm, which corresponds to the bands observed for the solid-state vis−NIR−IR spectrum of $[Bu_2Ph_2Tth]PF_6$. An increase in the loading from 5 to 15 wt % progressively shifts the bands from 1000 nm to 1100 nm and 1900 nm to 2000 nm.[24] Above 15 wt %, there is little change in peak position with increase in loading. A 10 wt % film which was half oxidized yielded a spectrum with the same NIR bands as the fully oxidized 5 wt % film.

The conductivities of the 5, 10, 15, and 20 wt % films were measured to be $< 10^{-7}$, $<10^{-6}$, 4×10^{-4}, and 7×10^{-4} S/cm, respectively. For a pure film of $[Bu_2Ph_2Tth]PF_6$ cast under similar conditions, the conductivity was measured to be 9×10^{-4} S/cm. Thus, the conductivity threshold for the films appears to be at about 15 wt % loading. All conductivities are electronic with no change in conductivity after several hours of passing current through the sample. Exposure of the films to air for 2 weeks made little difference in the measured conductivity. In addition, the conductivity of 10 and 20 wt % half-oxidized films is similar to that of the 5 and 10 wt % fully oxidized films, respectively. The similarity of the conductivity and vis−NIR−IR spectra for the 10 and 20 wt % half-oxidized films to that of the 5 and 10 wt % half-oxidized films, respectively, indicates that there is no mixed valence stack formation in these samples.

The X-ray powder diffraction pattern[24] of a 15 wt % $[Bu_2Ph_2Tth]^+$/PMMA sample exhibits several sharp lines overlapping with the broad diffraction from the amorphous PMMA network. The sharp diffraction lines correlate with the lines observed for solid $[Bu_2Ph_2Tth]PF_6$, which suggests that the same stack structure exists when embedded in a polymer (amorphous) matrix. The relative weak intensity of the diffraction lines for the films may be indicative of a lower crystallinity or to loss of intensity due to scattering by the amorphous network surrounding the crystallites.

Yellow films of Bu_2Ph_2Tth embedded in PMMA were also prepared. Under a microscope, the Bu_2Ph_2Tth is observed to form pockets of very fine, densely packed needles that are over 100 μm long. The X-ray powder diffraction pattern of the 10 wt % loading film shows sharp lines for the Bu_2Ph_2Tth crystallites which overlap with the broad diffraction from the amorphous PMMA network. The lines of the powder diffraction pattern correlate well with those for Bu_2Ph_2Tth, indicating the crystallites in the PMMA films have the same structure as the bulk solid.

Discussion

Stability of $[Bu_2Ph_2Tth]PF_6$. Millimolar quantities of $[Bu_2Ph_2Tth]PF_6$ can be synthesized in a pure form by either electrochemical or chemical oxidation to give highly reflective,

(24) See Supporting Information.

(25) The Miller indexes (*hkl*) and distance between adjacent planes based on the (*hkl*) values were determined from the equations governing the *d* spacing of the unit cell of each structure. In addition, the extinction conditions for the (*hkl*) values for the space group of each structure were used to eliminate those indexes which will give no diffraction lines. The equations for Bu_2Ph_2Tth are the following: orthorhombic unit cell, $(1/d^2) = (h^2/a^2) + (k^2/b^2) + (l^2/c^2)$. The extinction conditions for $Pca2_1$ space group are $(0kl)$ for $l = 2n + 1$, $(h0l)$ for $h = 2n + 1$, $(h00)$ for $h = 2n + 1$, and $(00l)$ for $l = 2n + 1$. For $[Bu_2Ph_2Tth]PF_6$ the equations are the following: monoclinic, $(1/d^2) = (1/\sin^2\beta)\{h^2/a^2 + (k^2 \sin^2 \beta/b^2) + (l^2/c^2 - 2hl(\cos \beta)/ac)\}$. The extinction conditions are (hkl) for $(h + k) = 2n + 1$, $(h0l)$, $(h00)$, or $(00l)$ for h, $l = 2n + 1$, and $(0k0)$ for $k = 2n + 1$. Equations and extinction conditions are taken from ref 15.

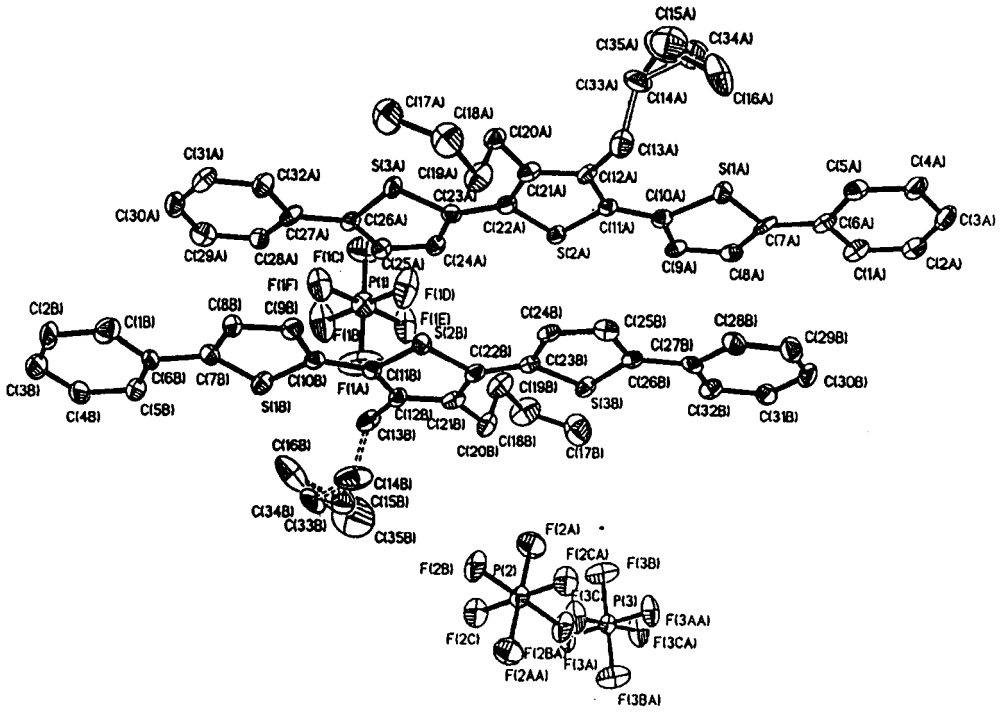

Figure 6. ORTEP diagram and atomic numbering for $[Bu_2Ph_2Tth]PF_6$ at 106 K. The asymmetric unit consists of both molecules.

dark purple needles or microcrystalline powders, respectively.[2] The two synthetic routes give solids with the same intrinsic structure as exemplified by the identical X-ray power diffraction patterns. The sharp diffraction lines and lack of amorphous reflections indicate that the solids are highly crystalline. The good correlation of the experimental and calculated powder diffraction lines indicate the bulk solid samples have the same structure as the single crystal studied. This is important as this packing structure appears to be dominant for our sample. The dominance of this structure is supported by the similarity of the X-ray powder diffraction patterns and UV−vis−NIR−IR spectra for the synthesized solids and the solution-cast films of $[Bu_2Ph_2Tth]PF_6$/PMMA.

The cation radical $[Bu_2Ph_2Tth]^+$ has a limited lifetime in solution before decomposition or reduction occurs. In dichloromethane, $[Bu_2Ph_2Tth]^+$ is stable at room temperature for several hours, while in acetonitrile, the oxidized form is stable for only an hour or two at room temperature. Hexafluoro-2-propanol solutions of $[Bu_2Ph_2Tth]^+$ give the best stability as solutions are stable for days *in air*. Lowering the solution temperature (<0 °C) increase the stability of $[Bu_2Ph_2Tth]^+$ so that it is stable for days or weeks depending on the solvent, dryness of the solvent, and quality of the inert atmosphere the sample is stored under.

X-ray Crystal Structures of Bu_2Ph_2Tth and $[Bu_2Ph_2Tth]PF_6$. The crystal structure of $[Bu_2Ph_2Tth]PF_6$ at 293 K was reported previously.[2] The crystal structures of Bu_2Ph_2Tth at 297 K and $[Bu_2Ph_2Tth]PF_6$ at 106 K were also obtained and are reported here. The three structures will be discussed and compared to highlight the important structural similarities and differences.

The X-ray crystal structure of the same crystal of $[Bu_2Ph_2Tth]PF_6$ studied at 293 K[2] was also determined at 106 K as variable-temperature UV−vis, ESR, conductivity, and X-ray crystallography studies indicated that the material may undergo a reversible phase transition. This was supported by the change in the unit cell constants for the material as the temperature was lowered from 293 K to 106 K. The change at lower temperature appears to give rise to a superlattice where there is a doubling of the *c* axis, unit cell volume, and number of molecules in the unit cell. The structure at 106 K shows similarities to that at 293 K, but there are also significant structural changes indicative of a phase transition (Figures 6 and 7). At 106 K each of the $[Bu_2Ph_2Tth]^+$ cations has thiophene rings with the transoid orientation for the sulfur atoms (as at 293 K). In addition, the thiophene and phenyl rings form a nearly perfectly planar molecule with deviations from the least-squares plane of less than 0.01 Å (as at 293 K). The 106 K structure also exhibits columnar stacks of $[Bu_2Ph_2Tth]^+$ cations and channels, which contain the PF_6^- anions. The columns lie along the needle axis of the crystals (the (001) direction) but the axis of the slipped π-stacking direction is at about a 45° angle to the (001) direction. In the 106 K structure, the $[Bu_2Ph_2Tth]^+$ columns have regular variations in the intermolecular spacings: the contact distance alternates regularly such that each cation has interplanar contact distances of 3.36(5) and 3.42(5) Å to the two neighboring cations in the π-stack. In effect, the 106 K structure has π-dimers that π-stack to form the columns in contrast to the infinite π-stacks of $[Bu_2Ph_2Tth]^+$ cations evenly spaced by 3.47 Å at 293 K. The description of the packing at 106 K as a "π-stack of π-dimers" is likely an oversimplification, but the regular variation in the intermolecular distances within the π-stacks has important implications for the properties for the compound at lower temperatures (vida infra). In the plane perpendicular to the stacking direction, the $[Bu_2Ph_2Tth]^+$ cations of the 106 K structure form sheets that exhibit no unusually close contacts between cations in the same layer. As at 293 K, the butyl groups are arranged to form the channels occupied by the PF_6^- anions but the butyl groups exhibit a greater degree of disorder at 106 K versus that at 293 K.

In addition to variations in the intermolecular contact distances, lowering the temperature leads to changes in the stacking arrangements of the molecules within a π-stack. At 106 K, the $[Bu_2Ph_2Tth]^+$ units overlap in a pseudo atom over atom type fashion where the three thiophene rings of a molecule lie directly in line with two of the thiophene rings and one phenyl ring of the adjacent molecules. In contrast, the 293 K

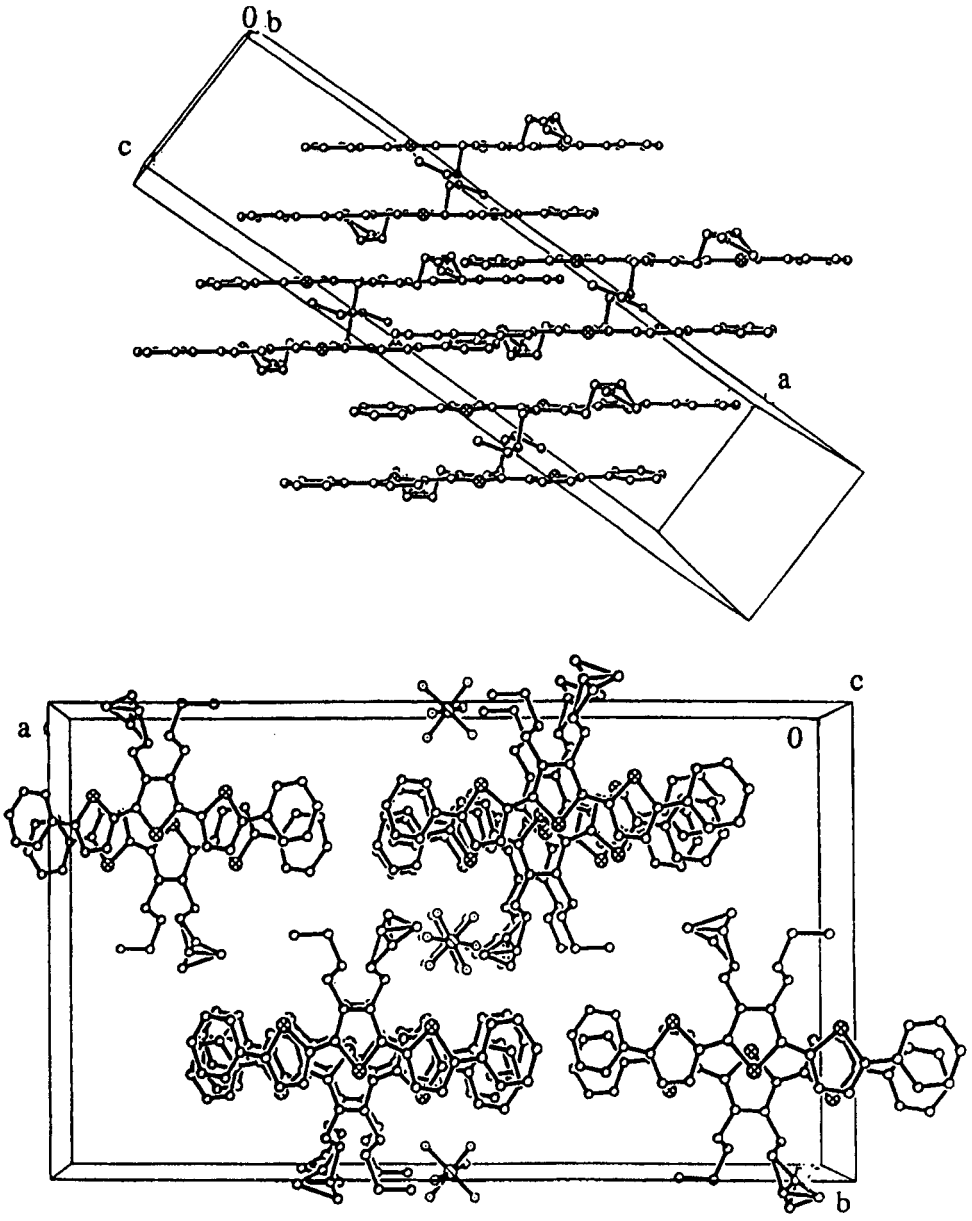

Figure 7. Two views of the packing structure of $[Bu_2Ph_2Tth]PF_6$ (at 106 K): (top) view parallel to the *ac* plane normal (PF_6^- anions left out for clarity) and (bottom) down the slipped packing direction (*c* axis).

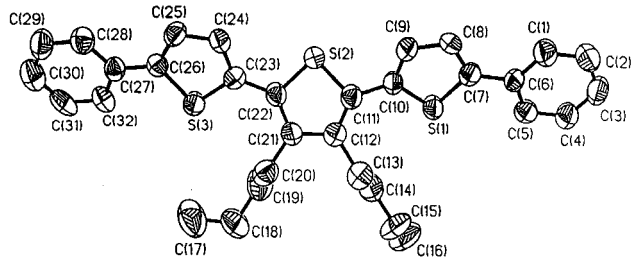

Figure 8. ORTEP diagram and atomic numbering scheme for Bu_2Ph_2Tth. The entire molecule is the asymmetric unit.

structure exhibits an atom over bond type overlap where the rings of adjacent molecules are slipped so that the center of each ring lies approximately in line with the C−C bond joining two rings of adjacent molecules.

The crystal structure of the neutral form Bu_2Ph_2Tth was also obtained (Figures 8 and 9). In this structure each of the Bu_2Ph_2Tth units adopts a transoid orientation of the sulfur atoms in adjacent thiophene rings. Each phenyl and thiophene ring of the Bu_2Ph_2Tth unit is planar within 0.01 Å, but in contrast to the oxidized structures, each Bu_2Ph_2Tth unit is nonplanar due to the ring twisting. The twist angles for the rings are 9° for the phenyl−thiophene rings of atoms S(1) and C(1−10); about 1° for the phenyl−thiophene rings with atoms S(3) and C(23−32); and about 34° and 26° for the twist angle of the middle thiophene ring to the rings with S(3)/C(23−26) and S(1)/C(7−10), respectively. The nonplanar Bu_2Ph_2Tth units form columnar "stacks" in which the atoms of each molecule lie almost directly above and below the equivalent atoms in the adjacent molecules. There are two separate stack types within the crystal which differ only with respect to their orientation: the normal of one π-stack makes a 74° angle to the normal of a neighboring π-stack. This packing motif is quite different from the typical herringbone type packing structure prevalent in the crystal structures of other neutral oligothiophenes.[11] The intermolecular spacing within a "stack" (measured as the distance between the middle thiophene rings of adjacent Bu_2Ph_2Tth units) is rather long at 4.71 Å. In contrast, the closest intermolecular contact distances between adjacent stacks are generally <4.0 Å. The overall packing efficiency of this structure (68%, calculated from the unit cell volume and the

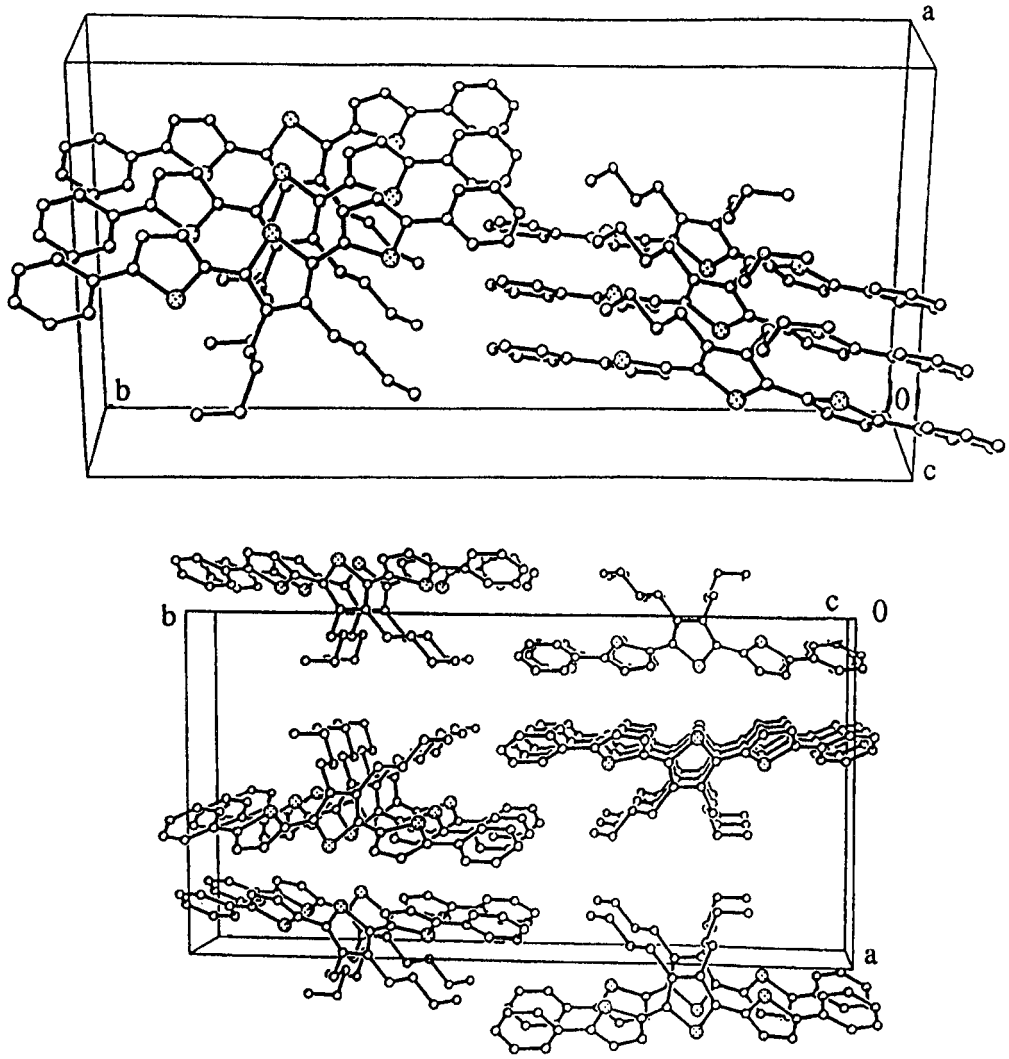

Figure 9. Two views of the packing structure of Bu_2Ph_2Tth: (top) view along the *c* axis and (bottom) parallel to the *ab* plane normal.

estimated molecular volume of each Bu_2Ph_2Tth unit (469.8 Å^3)[17]) is reasonable in comparison to other organic structures (65−75%).[26] The long intermolecular distance between molecules in a stack reflects poor packing *along* this direction. The forces associated with stacking appear to be less significant than those arising from interactions between stacks.

Selected bond lengths for the Bu_2Ph_2Tth and $[Bu_2Ph_2Tth]PF_6$ structures are shown in Table 4. Due to the large standard deviation in each value, quantitative comparisons of the data must be viewed with caution but general trends in the data are apparent. Several of the bond lengths significantly change upon going from the neutral to oxidized form, but there is little change in the bond lengths for the molecules of the oxidized form between 293 and 106 K. The C−C bond lengths of the thiophene rings change upon oxidation so that the "long" and "short" bonds of the neutral form become the "short" and "long" bonds of the oxidized forms, respectively. Furthermore, the thiophene ring C−C bond lengths become more similar in the oxidized forms than in the neutral form. The C−S bond lengths are very similar in all structures while the C−C bonds joining the thiophene rings are shortened in the oxidized forms. The two C−C bonds of the phenyls which involve the phenyl carbon (e.g. C(6)) bound to the carbon of the adjacent thiophene ring (e.g. C(7)) appear to lengthen upon oxidation whereas the rest of the C−C bonds of the phenyls are very similar in all the structures. These results indicate that the structural rearrangements that occur upon oxidation are largely localized on the thiophene rings and only two of the C−C bond lengths of the phenyl rings are slightly affected (those bonds adjacent to the thiophene rings).

The structures of Bu_2Ph_2Tth and $[Bu_2Ph_2Tth]PF_6$ at 297 and 106 K have several important similarities and differences. All three structures exhibit infinite stacks of molecules, but the molecular orientations, arrangements, and intermolecular overlap varies significantly. For example, each $[Bu_2Ph_2Tth]PF_6$ molecule is completely planar while the ring twists in Bu_2Ph_2Tth create nonplanar units. In the $[Bu_2Ph_2Tth]PF_6$ structures, the molecules form sheets corresponding to one row of each of the $[Bu_2Ph_2Tth]^+$ stacks while in the neutral form there are no sheets due to the different orientations of the stacks. The Bu_2Ph_2Tth columns consist of "stacking" molecules in the same orientation so that the equivalent atoms of adjacent molecules overlap while adjacent molecules of the oxidized forms have alternating orientations of adjacent molecules (i.e. the butyls are on opposite sides of adjacent molecules). The interplanar contact distance of the Bu_2Ph_2Tth units in a column (4.71 Å) is much larger than either the combined van der Waals radii of a carbon−carbon (3.3−3.4 Å)[27] or a sulfur−sulfur (3.45−3.5 Å)[27] interaction. The interplanar contact distance (3.47 Å) between the $[Bu_2Ph_2Tth]^+$ units at 293 K is slightly larger than the

(26) Kitaigorodsky, A. I. *Molecular Crystals and Molecules;* Academic Press: New York, 1973; pp 100 and 101.

(27) Bondi, A. *J. Phys. Chem.* **1964**, *68(3),* 441.

Table 4. Comparison of Selected Bond Lengths for Bu_2Ph_2Tth and $[Bu_2Ph_2Tth]PF_6$[a]

	Bu_2Ph_2Tth		$[Bu_2Ph_2Tth]PF_6$	
bond	at 297 K	at 297 K	at 106 K (**A**)[b]	at 106 K (**B**)[b]
phenyl rings				
C(1)−C(6)	1.372(10)	1.405(7)	1.416(7)	1.398(8)
C(1)−C(2)	1.389(11)	1.383(9)	1.374(7)	1.391(7)
C(2)−C(3)	1.359(12)	1.364(9)	1.388(8)	1.392(8)
C(3)−C(4)	1.353(12)	1.383(8)	1.397(8)	1.385(8)
C(4)−C(5)	1.380(11)	1.368(8)	1.366(7)	1.393(7)
C(5)−C(6)	1.370(10)	1.403(7)	1.414(7)	1.411(7)
thiophene rings				
C(6)−C(7)	1.478(9)	1.446(7)	1.433(7)	1.456(7)
C(7)−C(8)	1.358(10)	1.390(7)	1.395(7)	1.382(7)
C(8)−C(9)	1.401(10)	1.369(7)	1.379(7)	1.397(7)
C(9)−C(10)	1.356(10)	1.393(6)	1.414(7)	1.388(7)
C(10)−C(11)	1.468(10)	1.417(7)	1.423(7)	1.413(7)
C(11)−C(12)	1.362(10)	1.426(6)	1.418(7)	1.422(7)
C(12)−C(21)	1.439(9)	1.386(10)	1.397(7)	1.391(7)
S(1)−C(7)	1.724(8)	1.721(5)	1.742(5)	1.731(5)
S(1)−C(10)	1.730(7)	1.737(5)	1.739(5)	1.733(5)
S(2)−C(11)	1.725(7)	1.730(5)	1.741(5)	1.742(5)

[a] Numbering schemes are illustrated in Figures 6 and 8. The selected bond lengths are for only half of the molecule. The bond lengths for equivalent sites in the other half of the molecule are very similar to those listed and were left out for brevity. [b] This structure has two complete molecules (**A** and **B**) as the asymmetric unit. The values listed are the lengths for half of each of these independent molecules.

combined van der Waals radii of a carbon−carbon interaction and similar to that of a carbon−sulfur interaction. At 106 K, the interplanar contact distance between the $[Bu_2Ph_2Tth]^+$ dimers (3.36 Å) and dimer units (3.42 Å) is similar to the combined van der Waals radii of a carbon−carbon interaction (3.3−3.4 Å) and slightly smaller than that of a carbon−sulfur interaction (3.45−3.5 Å). Although the interplanar contact distance of the $[Bu_2Ph_2Tth]^+$ units in the oxidized forms is not particularly short, the *area of contact* between the molecules is large; thus it is likely that a significant degree of π-interaction is spread out over the molecules. For the 293 K structure, this π-interaction is equivalent between each cation, while at 106 K, this π-interaction varies so that it is strong between two molecules (3.36 Å) and slightly weaker (3.42 Å) between these molecules and adjacent ones in the π-stacks. The significant degree of intermolecular overlap in both structures is evidenced by the strong NIR−IR absorptions of $[Bu_2Ph_2Tth]PF_6$ which are characteristic of π-stacks.[4b,c,28]

The structural differences highlighted above are very important as the oxidized forms appear to have good intermolecular overlap, which allows for the formation of a π-network, while the neutral form does not. These structural differences also indicate that doping of the crystalline form of Bu_2Ph_2Tth *will not produce* the stacking characteristic of $[Bu_2Ph_2Tth]PF_6$ as there is too great of a structural rearrangement required. It is more likely that doping of the neutral form will lead to a derivative of the Bu_2Ph_2Tth structure, which has shorter intermolecular distances and different arrangements of the incorporated anions. Thus, the doping of Bu_2Ph_2Tth by iodine is expected to lead to a third phase of packing as is supported by the X-ray powder diffraction data for the I_2-doped Bu_2Ph_2Tth.

Electronic Structure of $[Bu_2Ph_2Tth]PF_6$ in Solution and the Solid State. In order to gain insight into the electronic structure of the solid-state forms of $[Bu_2Ph_2Tth]PF_6$, it is instructive to first consider the electronic structure of the monomeric and dimeric forms of $[Bu_2Ph_2Tth]^+$ in solution. The

(28) Miller, L. L.; Zhong, C.-J.; Kasai, P. *J. Am. Chem. Soc.* **1993**, *115*, 5982.

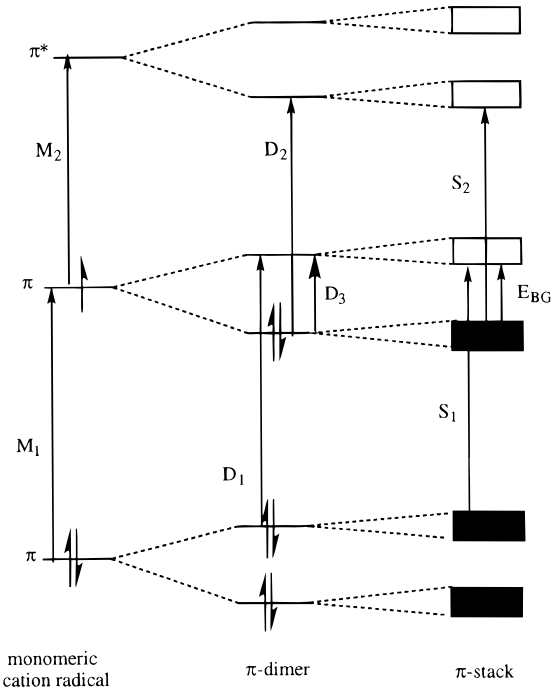

Figure 10. Qualitative MO diagram for the monomeric, dimeric, and π-stacked forms of $[Bu_2Ph_2Tth]PF_6$ in solution and the solid state.

results of the optical and electrochemical studies support the formulation of $[Bu_2Ph_2Tth]PF_6$ in solution as a cation radical and PF_6^- anions. The frontier MO diagram for a $[Bu_2Ph_2Tth]^+$ radical cation is shown in Figure 10.[5a] The low- and high-energy bands for monomeric $[Bu_2Ph_2Tth]^+$ are assigned as the transitions E_{M1} and E_{M2}, respectively. Upon π-dimerization, the orbitals of two monomeric molecules overlap to give the diagram shown in Figure 10. The three bands of the π-dimer are thus assigned as the transitions E_{D1}, E_{D2}, and E_{D3} where the energy follows the trend $E_{D1} > E_{D2} > E_{D3}$. The ESR silence of the π-dimer is a direct result of the π-dimerization as this leads to pairing of two unpaired electrons from different molecules. The physical structure of this π-dimer is unknown, but it is likely to have similar features to those observed for the $[Bu_2Ph_2Tth]PF_6$ X-ray structures.

There is also an interest to determine to what extent, if any, the phenyl rings are conjugated to the thiophene rings. This analysis compares the electrochemical and optical properties of Bu_2Ph_2Tth and $[Bu_2Ph_2Tth]^+$ to those of related alkylated oligothiophenes. Two series of oligothiophenes with three, four, and five thiophene rings that have (1) either methyls capping the α-position (α-Me)[7a] or (2) a hexyl chain bridging the α and β positions of the end thiophene rings (α,β-Hx)[18] were used. The λ_{max} for the $\pi-\pi^*$ band of neutral Bu_2Ph_2Tth (384 nm) is closer to those alkylated oligothiophenes with three thiophene rings (363 nm for α-Me; 375 nm for α,β-Hx) than those with four (397 nm for α-Me; 410 nm for α,β-Hx) or five (422 nm for α-Me; 432 nm for α,β-Hx) rings. The center of the emission (λ_{em}) of Bu_2Ph_2Tth is closer to that for the α,β-Hx oligothiophenes with three rings (450 nm) than four (496 nm) and five (530 nm) rings. The location of the two main vis−NIR bands for monomeric $[Bu_2Ph_2Tth]^+$ is more similar to that of the alkyl substituted oligothiophene cation radicals with three (579, 886 nm for α-Me; 620, 939 nm for α,β-Hx) and four (670, 1117 nm for α-Me; 693, 1181 nm for α,β-Hx) thiophene rings than those with five rings (747, 1348 nm for α-Me; 725, 1252 nm for α,β-Hx). Thirdly, the first oxidation of Bu_2Ph_2-Tth is more similar to that of the three ring α-Me oligothiophene (1.02 V) than the four (0.84 V) and five (0.86 V) ring analogs.

The oxidation of Bu_2Ph_2Tth occurs at much higher potentials than for the α,β-capped alkylated oligothiophenes with three, four, or five rings (0.38, 0.32, and 0.26 V vs ferrocene, respectively). The lower oxidation potentials of the α,β-Hx than the α-Me analogs likely result from the unique substitution of the α and β positions in the α,β-Hx molecules. The similarity of the oxidation potentials λ_{max} and λ_{em} for $Bu_2Ph_2Tth/[Bu_2Ph_2Tth]^+$ and the three ring alkylated oligothiophenes indicates that the phenyls weakly affect the spectral properties. On the basis of this analysis, it appears that $[Bu_2Ph_2Tth]^+$ has the positive charge mainly localized on the oligothiophene portion and that the phenyl groups are largely substituents. This also appears to be the case in the solid state as the room temperature X-ray crystal structures of the neutral and oxidized forms of Bu_2Ph_2Tth exhibit only minor differences in the C−C bond lengths of the phenyl rings while the C−C bond lengths of the thiophene rings exhibit more significant changes.

The electronic structure of $[Bu_2Ph_2Tth]PF_6$ in the solid state is of even greater interest. $[Bu_2Ph_2Tth]PF_6$ forms infinite π-stacks at room temperature and "π-stacks of π-dimers" at lower temperatures. These structures should lead to band type electronic structures, and variable-temperature UV−vis−NIR, ESR, and conductivity studies support this hypothesis. The conductivity values are typical of a semiconductor[29] and decrease with temperature. This temperature dependence is characteristic of semiconductors, but in this case, the dependence is also related to structural changes. The observed decrease in ESR signal intensity at low temperatures is also consistent with a semiconductor band structure.

The UV−vis−NIR spectra of solid samples of $[Bu_2Ph_2Tth]PF_6$ are also consistent with a semiconductor band structure and the transitions can be assigned to E_{S1}, E_{S2}, and E_{BG} in Figure 10. Thus the NIR transition energy correlates with the energy of the band gap.[28] The NIR transition shifts from 1920 nm at 290 K to 1780 nm at 190 K. This shift correlates well with the structural change observed by X-ray crystallography where at lower temperature there is a conversion from infinite π-stacks to "π-stacks of π-dimers." This structural change will lead to a larger band gap and higher energy NIR absorption due to weaker long-range interactions in the π-stacks. The dependence of the optical conduction band on the weight percent loading of the $[Bu_2Ph_2Tth]^+$/PMMA films is also consistent with the semiconductor theory. For these films, the NIR absorption shifts to lower energy as the loading is increased from 5 to 15 wt %. This shift appears to be associated with a larger degree of π-stacking in the higher weight percent samples (i.e. lower energy E_{BG}).

It might be expected that conductivity would be higher along the stack direction. Interestingly, this could not be unambiguously determined for our system as face indexing of the crystals shows that the needle axis (the (001) direction) is at about a 45° angle to the axis of the slipped π-stack direction. Therefore, the conductivity measured along or across the needle axis will be the sum of the components for conduction *between* π-stacks and *through* π-stacks.

(29) Lider, D. R., Ed. *Handbook of Chemistry and Physics, 71st ed.;* CRC Press: Boston, 1990; pp **12**-23, **12**-63.

Conclusions

The crystal structure of $[Bu_2Ph_2Tth]PF_6$ was determined at 293 and 106 K. At 106 K, $[Bu_2Ph_2Tth]PF_6$ forms a superlattice where the *c* axis is approximately double that at 293 K. The 106 and 293 K structures of $[Bu_2Ph_2Tth]PF_6$ have similar π-stacking ("slipped stacks" of $[Bu_2Ph_2Tth]^+$ cations), but the overlap between adjacent molecules (distances and orientations) is significantly different. These structural changes likely play an important role in the temperature dependence of the physical properties of the bulk material. Comparison of the crystal structure of Bu_2Ph_2Tth and $[Bu_2Ph_2Tth]PF_6$ shows that doping of the crystalline form of Bu_2Ph_2Tth will not produce the structure of $[Bu_2Ph_2Tth]PF_6$ as there is too great of a structural rearrangement required. The results of the physical studies of the solution, solid-state, and polymer-embedded samples of $[Bu_2Ph_2Tth]PF_6$ are correlated to the physical structures of these forms; these results indicate the solid-state material has a semiconductor band structure. The physical and electronic structure for $[Bu_2Ph_2Tth]PF_6$ appears to be highly favorable as X-ray powder diffraction and vis−NIR studies indicate that this structural motif is dominant in the chemically oxidized and electrocrystallized samples as well as in the $[Bu_2Ph_2Tth]PF_6$/PMMA films. This work also strongly supports a conduction mechanism *through the* π-stacks and not between π-stacks: the polaron/bipolaron theory does not adequately model this system. In conclusion, π-stacks and π-interactions are important mechanisms for conduction in $[Bu_2Ph_2Tth]PF_6$ and are expected to be important in other oxidized oligomer and polymer systems.

Acknowledgment. This research was supported by the National Science Foundation under Grant No. CHE-9307837. We would like to thank Dr. Victor G. Young, Jr., for help in solving the crystal structures. D.D.G. thanks the National Science Foundation for a Pre-Doctoral Fellowship.

Supporting Information Available: Full details of the X-ray crystal structures of Bu_2Ph_2Tth and $[Bu_2Ph_2Tth]PF_6$ at 106 K including structure determination summary and tables listing positional parameters, isotropic and anisotropic displacement parameters and bond lengths and angles, tables of indexed X-ray powder diffraction lines for Bu_2Ph_2Tth and $[Bu_2Ph_2Tth]PF_6$, X-ray powder diffraction figures for electrocrystallized $[Bu_2Ph_2Tth]PF_6$, Bu_2Ph_2Tth doped with I_2, and 20 wt % $[Bu_2Ph_2Tth]PF_6$ in PMMA, and vis−NIR−IR spectra of 5, 10, and 15 wt % $[Bu_2Ph_2Tth]PF_6$ in PMMA (41 pages). See any current masthead for ordering and Internet access instructions.

JA964345M